Energy 198 (2020) 117377

Contents lists available at ScienceDirect

Energy

journal homepage: www.elsevier.com/locate/energy

Optimization of the operating conditions of a beta-type rhombic drive stirling engine by using response surface method

Hamit Solmaz [a,*], Seyed Mohammad Safieddin Ardebili [b], Fatih Aksoy [c], Alper Calam [d], Emre Yılmaz [e], Muhammed Arslan [f]

[a] Automotive Engineering Department, Faculty of Technology, Gazi University, Ankara, Turkey
[b] Department of Biosystems Engineering, Shahid Chamran University of Ahvaz, Ahvaz, Iran
[c] Department of Automotive Engineering, Faculty of Technology, Afyon Kocatepe University, Afyon, Turkey
[d] Machinery and Metal Technologies, Technical Sciences Vocational High School, Gazi University, Ankara, Turkey
[e] Department of Automotive Technology, Arifiye Vocational High School, Sakarya University of Applied Science, Sakarya, Turkey
[f] Automotive Technologies, Çay Vocational High School, Afyon Kocatepe University, Afyon, Turkey

ARTICLE INFO

Article history:
Received 8 December 2019
Received in revised form
27 February 2020
Accepted 11 March 2020
Available online 13 March 2020

Keywords:
Stirling engine
Performance optimization
Charge pressure
Heating temperature
Response surface method

ABSTRACT

The aim of this paper is to provide a multi-objective model to evaluate the effect of engine working parameters on the performance characteristics of a beta-type Stirling engine. The second objective of the study is to enhance the specific power of the engine, which was designed and manufactured in a previous study, via increasing the compression ratio. The selected independent variables were: charge pressure (2–9 bar), heating temperature (500–700 °C), and engine speed (550–750 rpm). The engine was analysed using the design of experiments based on the response surface method, and the most appropriate model was achieved. The desirability function approach was used to determine the optimum engine working condition. Optimal engine speed, charge pressure, charge pressure were 700 rpm, 8 bar, and 700 °C, respectively, with the desirability value of 0.86. At optimal engine working conditions, the amounts of the brake torque and brake power were found to be 11.95 Nm and 868.13 W, respectively. Optimized parameters are then compared and validated against the experimental data of the Stirling engine with an error of 4%. The specific power of the engine was found to be 1100 W/L which is 13% higher than the previous design.

1. Introduction

Energy demand is increasing over the world day by day, and most of this demand is still compensated via fossil fuels. The use of fossil fuels leads to an increasing environmental concern because of the harmful exhaust gases to human health and greenhouse gas of CO2 which responsible for climate change [1–7,74,75]. To eliminate the harmful effects, renewable biofuels seem to be an alternative to reduce the consumption of fossil fuels. For this reason, many studies have been carried out about alternative fuels such as biodiesel, ethanol methanol, etc. [8–15,76,77]. However, the current energy conversion efficiency of the internal combustion engines, which can be powered with alternative fuels, is not at an acceptable level. Low-temperature combustion modes such as HCCI, RCCI, PCCI etc. are promising technologies to obtain higher thermal efficiency and lower soot and NOx emissions from internal combustion engines but these technologies are still in development and couldn't use for industrial applications [16–20]. Therefore, high energy conversion efficiency systems are required to meet energy demand and reduce environmental impacts simultaneously.

Stirling engines take attention due to their high energy conversion efficiency level. The thermal efficiency of the regenerative Stirling cycle is equal to Carnot efficiency [21,22]. The history of Stirling engines based on 200 years ago, so appeared earlier than the petroleum engine (1860), electric motor (1869), and diesel engine (1893) [23,24]. Stirling engines, which were firstly named hot air or hot gas engine, were invented by Robert Stirling in 1816 and used to prevent the explosion hazard of steam engines [25,26]. Because Stirling engines are external combustion engines and capable to run at low pressures [27]. Another attractive

* Corresponding author.
E-mail addresses: hsolmaz@gazi.edu.tr (H. Solmaz), m.safieddin@scu.ac.ir (S.M. Safieddin Ardebili), faksoy@aku.edu.tr (F. Aksoy), acalam@gazi.edu.tr (A. Calam), emreylmz@gazi.edu.tr (E. Yılmaz), muarslan@aku.edu.tr (M. Arslan).

https://doi.org/10.1016/j.energy.2020.117377
0360-5442/

Nomenclature

RSM	response surface method
DF	desirability function
CCD	central Composite design
f	response function
CO_2	carbon dioxide
NOX	nitrogen oxides
CFD	computational fluid dynamics
HCCI	homogeneous charge compression ignition
RCCI	reactivity controlled compression ignition
PCCI	premixed charge compression ignition
FPSE	free-piston Stirling engine
ANOVA	analysis of variance
ε	error
df_n	overall desirability
Pi	importance of each factor
y_i	response value
w_i^{max}	maximum values for the response
w_i^{min}	minimum values for the response

specification of the Stirling engine is the flexibility of the required energy source to run the engine. Many renewable energy resources such as solar, geothermal, biomass and waste heat can be used to run Stirling engines [28,29].

Stirling engines are classified into two groups as kinematic engines and free-piston engines according to their drive mechanisms. In kinematic engines, the synchronization of the displacer and the power piston is provided by a drive mechanism such as slider-crank drive mechanism, rhombic drive mechanism, ross yoke mechanism, etc. [30–34]. In free-piston engines, the power piston and displacer have no mechanical connection and movement is ensured by the pressure difference and the stiffness of the springs [35]. There are three types of cylinder configuration used in Stirling engines. Alpha configuration has two pistons, working at separate cylinders [36]. In the beta arrangement, a displacer and a piston operate at the same cylinder [37] while both of them work at separate cylinders in gamma cylinder arrangement [38]. Among all of these configurations, the beta-type rhombic drive Stirling engine stands out due to its high power level [39,40].

The rhombic drive mechanism, which was firstly used by R.J. Meijer in 1953 for a beta type Stirling engine, has low vibration and noise levels [41,42]. It is generally used in beta type engines, and the piston rod of displacer extends inside of the power piston. Owing to the fact that piston and displacer work at the same axial, there is no need for lubrication [43]. Also, lateral forces are mutually balanced, so it assures low friction and wear. Therefore, the rhombic drive mechanism is used to decrease friction between the moving components, remove efficiency losses caused by frictions and obtain higher power from little size engines [44]. Many studies had been conducted to design, and manufacture the rhombic drive beta type Stirling engine till today. For instance, MAN (Maschinenfabrik Ausburg-Nürnberg) and MWM (Motorenwerke Mannheim), designed and manufactured a 22 kW Stirling engine with the rhombic drive mechanism called as 1–400 model. General Motors and Philips companies designed and built a PD-46 model 3 kW solar-powered Stirling engine with a rhombic drive mechanism for American Air Forces to use in space applications [45]. In 1958, General Motors [44] manufactured a single cylinder 1–98 model 7,3 kW Stirling engine with the rhombic drive mechanism.

Optimization studies on beta type rhombic drive Stirling engine were mostly focused on determining the dimensions of the engine. In those studies, it was aimed to obtain high power levels as possible by performing dimensionless, dynamic, and thermodynamic analyses. In a study, Cheng and Yu [43] aimed to prepare a theoretical model for a beta type Stirling engine with a rhombic drive mechanism. The effect of physical and geometrical parameters on the engine power and efficiency was investigated. Results showed that optimizing effective parameters such as distance between gears, regenerative gap, heat source temperature, etc. enhanced the engine performance. When the regenerative gap was 0.00005 m, the power of baseline cases reached a peak value of 16.75 W and provided 13.1% thermal efficiency. Also, when the heat source temperature reached from 600 K to 1200 K, power reached from 7.96 W to 32.78 W. Furthermore, when an increase of distance between centers of gears decreased output power and efficiency, but an increase of offset distance from crank to center of gear increased output power and efficiency. In a different study, Shendage et al. [46] studied on the design methodology and phase angle optimization of a beta type Stirling engine. In the study, the optimization was based on the numerical thermodynamic analysis. According to their results obtained, it was concluded that the eccentricity ratio of 1.5 was optimum value, but more eccentricity ratio would harm engine parts. Also, the Stirling engine with a rhombic drive mechanism provided about 10% more engine power compared to the Stirling engine with the crank drive mechanism, having the same sizes and working at the same conditions. El Hassani et al. [47] theoretically studied a solar-powered beta type Stirling engine with a rhombic drive mechanism. Also, theoretical thermodynamic optimization was performed. Dead spaces were also considered in the model to estimate engine performance. Their finding indicated that offset distance from the gear center to gear radius of the rhombic drive mechanism had to be maximized. On the other hand, other parameters had to be minimized. It was finally seen that engine power could be obtained as about 50% more with optimization.

Later in 2014, Cheng and Yang [48] optimized a beta type Stirling engine with a rhombic drive mechanism to maximize engine power with the dimensionless model. According to conclusions, it was seen that the theoretical model verified the experimental data with a 5.2% deviation. Zainudin et al. [49] developed a numerical model to predict the performance of a beta type Stirling engine with a rhombic drive mechanism. The conclusions showed that engine performance could be increased with the temperature difference between the heat source and sink. In addition, owing to the fact that the increase of working fluid pressure meant increasing of working fluid mass, high pressure increases absorption and rejection of energy. According to numerical modeling, the engine power was found to be 805 W at 300 rpm. Ni et al. [50] designed a beta type Stirling engine with a rhombic drive mechanism and designed a thermodynamic model named Improved Simple Analytical Model (ISAM) to predict engine performance. A 100 W beta type Stirling engine was experimentally tested with helium and nitrogen as the working fluid at 1.6–3 MPa pressures and 260–1380 r/min rotary speeds. According to experimental conclusions, maximum cycle efficiency and maximum engine power were obtained as 16.5% and 165 W with helium at 1120 r/min and 2.96 MPa. The ISAM confirmed the experimental data with a deviation of 1–7.1 for nitrogen and 4.3–13.4% for helium. In a different investigation, Badr et al. [51] simulated and optimized a beta type Stirling engine with a rhombic drive mechanism using MSC ADAMS software. Gas forces, masses, friction forces at the joints, inertias, temperatures of compression and expansion spaces were considered in the model. Optimization was carried out by taking account dynamic model of engine, and it was seen that engine power increased from 42.5 W to 135 W with optimization. Similarly, Xiao et al. [52] studied a beta type Stirling engine with a rhombic drive mechanism to develop a

methodology for optimization of geometric design and aimed a combined method for multi-objective optimization of the engine using data of pressure and volume obtained by Computational Fluid Dynamics (CFD) analysis. CFD analysis contains parameters such as matrix mesh, regenerator length, wire diameter. When dead volumes of the regenerator, heater, and cooler were decreased to 54%, 42%, and 24%, respectively, two percentage increase in thermal efficiency and more than 80 W at engine power were observed.

Yang and Cheng [53] aimed to design a theoretical model that can predict the performance better for a 500 W beta type Stirling engine with a rhombic drive mechanism. By taking into consideration the mechanical loss and pressure drop in all working spaces, it was determined that the shaft power was being predicted better, especially at high engine speeds. Theoretical findings were similar to experimental results in some particular cases. So, the improved engine produced 556 W engine power at a heating temperature of 1100 K and an engine speed of 1665 rpm. In another study, Yang et al. [54] aimed to develop a theoretical model to predict the dynamic behavior of a 1 kW beta-type Stirling engine with a rhombic drive mechanism. All friction losses were considered in the theoretical model. A prototype engine was built and tested to validate the theoretical model. It was concluded that the theoretical model jointly agreed with experiments. The maximum engine power was 1358 W at 1313 rpm.

Mohammadi and Jafarian [55] developed a second-order thermodynamic CFD model for the GPU-3 Stirling engine produced by General Motors. The data obtained from the model were compared with the data obtained from experiments. In order to see the effect of hydrodynamic losses on engine performance, losses such as mass leakage, regenerator ineffectiveness, shuttle effect, and mechanical frictions were ignored. It was found that the CFD model verified by the experiments with an error of 15.1%. In a different study, Ahmed et al. [56] developed a practically feasible thermodynamic model that incorporates power and thermal losses for beta type Stirling engine with a rhombic drive mechanism. Various parameters such as swept volume, temperature ratio, phase angle, regenerator matrix porosity, engine frequency, and the pressure were studied and optimized. The optimized model was finally compared with experimental data obtained from General Motor's prototype of the GPU-3 Stirling engine. The thermodynamic model efficiency was different by 1.56% from experimental efficiency so that power and efficiency increased by being optimized parameters. In a very recent study, Elghafour et al. [57] performed a three-dimensional CFD simulation for the GPU-3 engine. The effect of thermodynamic and fluid dynamic on the heat transfer event through a cycle were investigated. The results showed that the deviation between CFD data and experimental data was approximately 4%. Cheng et al. [58], developed, tested a 300 W beta type Stirling engine with a rhombic drive mechanism, and built a theoretical model to estimate engine performance. In replicated experiments, shaft power and thermal efficiency were 390 W and 32.2% at 1400 rpm, charged pressure of 8 bars, and heating temperature of 850 °C with a No. 120 wire mesh. The power data obtained from the theoretical model was 12–20% higher than the experimental power data.

The optimization studies were mostly focused on determining the dimension parameters of the Stirling engine, as it can be seen so far from the review above. In addition, a large part of those optimization studies was based on numerical thermodynamic analyses instead of a mathematically based optimization technique. However, practical operating parameters such as engine speed, charge pressure, hot and cold end temperatures, etc. have a significant impact on the engine performance for real-life applications. Statistical techniques based on experimental data and considered multi-variable presents better performance than empirical thermodynamic optimization techniques. One of the widely used optimization technique is the response surface method (RSM), which is a combination of statistical and mathematical methods [59–61]. It is possible to reach numerous RSM optimization studies conducted on internal combustion engines. Most of them focused on enhancing engine performance, reducing exhaust emissions, determining the optimal fuel blend and the optimal fuel production process [59–64]. Contrary to this, there are only two Stirling engine studies that benefited from RSM. One of them was performed by Gheith et al. [65] to optimize the operating parameters such as flow rate of cooling water, initial charge pressure, operation duration and heating temperature to enhance the power output of a gamma type Stirling engine. The experimental design was conducted with a central composite rotatable design approach by using five levels for these four parameters. According to optimization results, optimal operating conditions to obtain maximum engine power output of 355 W were found to be 8 bar charge pressure, 7.3 L/min cooling water flow and 500 °C heating temperature. Ye et al. [66] used RSM to optimize the performance of a free-piston Stirling engine (FPSE). Both the operating and structural parameters for FPSE were optimized. Optimization results for charge pressure, operating frequency, hot end and cold end temperature, length of cooler and heater, fin thickness of cooler and heater, phase angle were determined as 3.98 MPa, 84.93 Hz, 920 K, 330.3 K, 0.02 m, 0.017 m, 0.0008 m, 0.004 m and 80.78° respectively.

The above review reveals that the operating parameters have a significant impact on engine performance, and there is no study about the optimization of a beta-type Stirling engine before. In the present study, it was aimed to optimize the operating parameters of a beta-type rhombic drive Stirling engine by using the RSM. The rhombic drive mechanism of the engine used in this study was the same as the study performed by Aksoy et al. [67]. The second goal of this study is to enhance the specific power level of the engine by designing and manufacturing a new displacer and displacer cylinder assembly to increase the compression ratio of the engine.

2. Experimental setup

2.1. Stirling engine

The rhombic drive Stirling engine consists of a drive mechanism and a cylinder assembly. The drive mechanism of the engine, which was assembled in the main block, includes rhombus rods, linkage elements, helical gears, crankshafts, and bearings. The engine block was manufactured by C1040 material via welding, and six sides of the main body were covered. The covers supporting the bearings were manufactured by C1040 material. The remaining covers were manufactured by aluminum 5050 to reduce weight. The main block was grinded smoothly and oring canals placed on the covers to prevent gas leakages. Because of the high load and speed capacities and to provide silent working, helical gears were used on the rhombic drive mechanism. Helical gears were manufactured by case hardening steel, and hardening to 52 Rockwell C was applied. Helical gears were placed on crankshafts which were manufactured by C4140 material. Aluminum 7000 was used to manufacture the Rhombus rods. The drive mechanism and the lower part of the engine presented here are the same with the study conducted by Aksoy et al. [67]. Fig. 1 illustrates the drive mechanism.

The upper section of the engine consists of a power piston and its cylinder, displacer, displacer lower cylinder, and upper cylinder of the displacer. Fig. 2 shows the assembled version, schematic view, and displacer driving mechanism of the test motor. In rhombic drive, Stirling engines, the space between power piston and displacer is the cold volume, and the space above the displacer is hot volume. The hot and cold volumes are separated by a ring placed on the displacement piston. The flow of the working

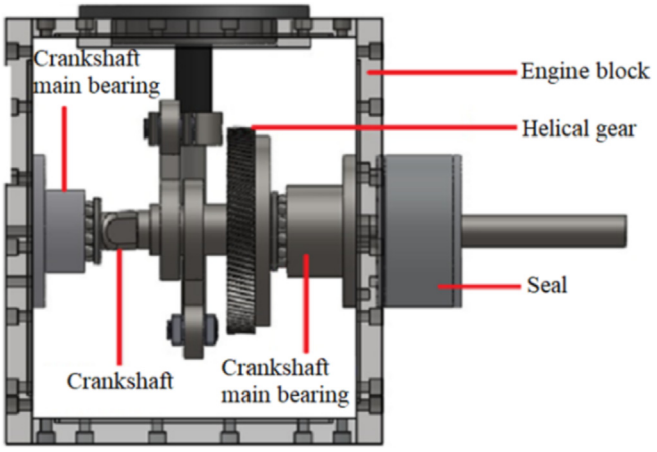

Fig. 1. Engine block and drive mechanism.

medium between the hot and cold volumes takes place from the regenerator volume in the displacer bottom cylinder. The regenerator material is placed between the displacer bottom cylinder and the power cylinder upper part.

The power cylinder and upper part of it were manufactured 8620 hardening steel. 70 cooling channels, 3 mm wide, 8 mm long, and 45 mm deep, were opened into the power cylinder and the upper part of the power cylinder. In order to increase the cooling performance and reduce the dead volume, 70 copper bars with 3 mm wide, 5 mm long, and 45 mm deep were inserted into these channels. The power piston was made of 7000 series aluminum, and there was a working gap of 0.07 mm between the power cylinder and the power piston. The displacer rod, which was made of mercury steel, passes through the center of the power piston, and a working gap of 0.03 mm was left between the two parts. The upper part of the power piston was constructed in steps to facilitate the flow of the working fluid. The cooler was made of aluminum material, and to increase the heat transfer surface areas, the inner side of it was grooved.

The displacer consists of two parts, the dome, and the lower part. In the previous version of the engine, the length of both the upper displacer cylinder and the displacer were longer compared to this study. The compression ratio of the engine was 2.51 in the previous engine configuration [67]. The compression ratio of the presented engine is 2.76 after shortening the displacer cylinder and the displacer length. Table 1 depicts the dimensions of the displacer and displacer cylinder. Other specifications of the engine can be found in the previous study [67]. The bottom part is made of stainless 304 material. A ring made of for cast material was used on the lower part to prevent leakage. The displacer dome was made of stainless ASTM 304 pipe with a wall thickness of 1.5 mm because of its low heat transfer coefficient and reduced heat transfer. A working gap of 0.7 mm was left between the displacer dome and the cylinder. The displacer cylinder is made of stainless ASTM 304 steel in two parts, top, and bottom. In order to increase the heat transfer during the transfer, 80 channels of 3 mm depth and 2 mm width were grooved on the inner surface of the displacer cylinders. Because of the shortening of the displacer cylinder, the heat transfer surface area on the displacer cylinder decreased by almost 20% in comparison with the previous study.

2.2. Experimental procedure and instrumentation

The performance of the prototype Stirling engine was tested at hot end temperatures of 500, 600, and 700 °C. In order to be sure that the air in the engine is fully evacuated, the engine block was filled with helium, the engine was operated 2 min and then discharged again and refilled. This procedure repeated 5 times. The engine was started to idle run at almost 350 °C hot end temperature with a charge pressure of 2 bar. However, initial experiments were performed with a hot end temperature of 500 °C because there was no significant power production below that temperature, especially for lower charge pressures of 2–4 bar. Working fluid charge pressure varied between 2 and 9 bars incrementally. To avoid any gas leakage, maximum charge pressure was limited to 9 bar. For each test case, the engine was allowed to run at its maximum speed freely for a while and then an external load was applied gradually to the flywheel to slow down the speed and measure the engine torque. In order to reduce the measurement error, each test case was repeated three times.

A schematic view of the testbed is shown in Fig. 3. The charge pressure was measured by a digital pressure gauge, which has an accuracy value of 0.01 bar, placed on the engine block. The hot-end temperature was kept constant by setting the gas flow of liquid

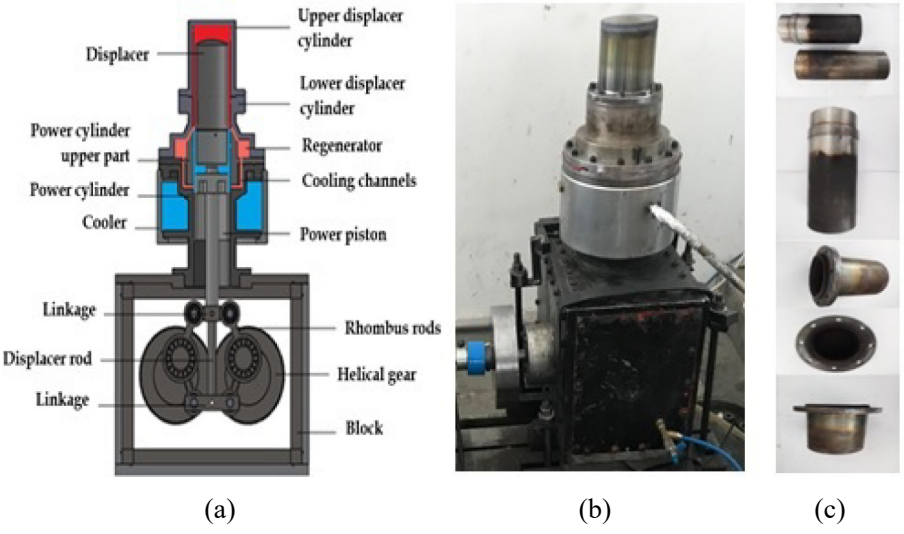

Fig. 2. (a) Schematic view of the beta type rhombic drive Stirling engine (b) manufactured Stirling engine, and (c) displacer driving mechanism.

Table 1
Some specific properties of the engine.

Characteristics	Previous design [67]	This study
Displacer length [m]	0.285	0.213
Length of upper displacer cylinder [m]	0.180	0.110
Compression ratio	2.51	2.76

Table 2
Accuracy of the equipment and uncertainties of the calculated values.

Measurement	Accuracy	Calculated Uncertainty
Engine Torque	±0.05 kg (from load cell)	±0.017 Nm
Engine speed	±1 rpm	–
Engine Power	–	0.3% - 0.7%
Temperature	±1.5 °C	–

petroleum gas (LPG) burner. ESIT BB20 brand load cell was used to measure engine torque with an accuracy of ±0.05 kg. Cold and hot end temperatures were measured with TMS DT-8859 infrared thermometer and NiCr−Ni type thermocouple. Engine speed information was obtained by using a 5000 pulse encoder. Engine speed and torque were recorded on the computer by utilizing a data acquisition card. Uncertainties were calculated with the root square method presented by Kline and McClintock [68]. For the uncertainty of the engine power, an error range between minimum and maximum was given because the engine speed has a range. Uncertainties of the calculated values and the accuracy of the measurement equipment is given in Table 2.

2.3. Experimental design

This section deals with the determination of optimum engine performance conditions for maximizing the engine brake power and minimize the hot-end temperature. The optimization of independent parameters was carried out by using the Response surface methodology (RSM).

The RSM technique offers some advantages in comparison with full factorial design experimentation, such as requiring fewer tests and less time-consuming [61].

The Response surface model can be described by its general form for modeling the dependent variable Y which is influenced by a number of independent parameters x_1, x_2, …,x_n [69].

$$Y = f(X_1, X_2, \ldots, X_n) + \varepsilon \quad (1)$$

where f is the response function, and ε denotes the error associated with the experiments. In the RSM method, a multiple regression analysis is determined for response parameters that represent the interaction and the main effects of input variables on each response separately. Fig. 4 illustrates the different stages of Stirling engine performance optimization based on the independent and response variables using RSM techniques.

In this research, the central composite design (CCD) method was

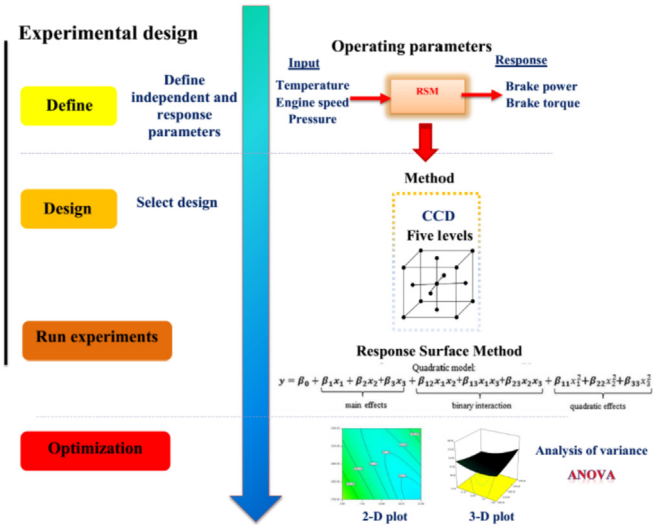

Fig. 4. Design of experiment (DoE) for Stirling engine performance in RSM.

employed to evaluate the effect of engine speed, charge pressure, and temperature as input parameters on the engine performance, including engine torque and brake power. For this purpose, engine speed, charge pressure, and temperature were chosen as the independent parameters, and the output factors were engine brake power and torque as the response parameters (Table 3).

The Design Expert v.10 was used to analyze the fitness and the significance of the DoE model to derive the best equation between the input and the output parameters. Besides, the analysis of variance (ANOVA) manifests the effect of independent parameters on each response variable.

The simultaneous optimization was performed by combining all responses into a desirability function (DF) using the following equation [70].

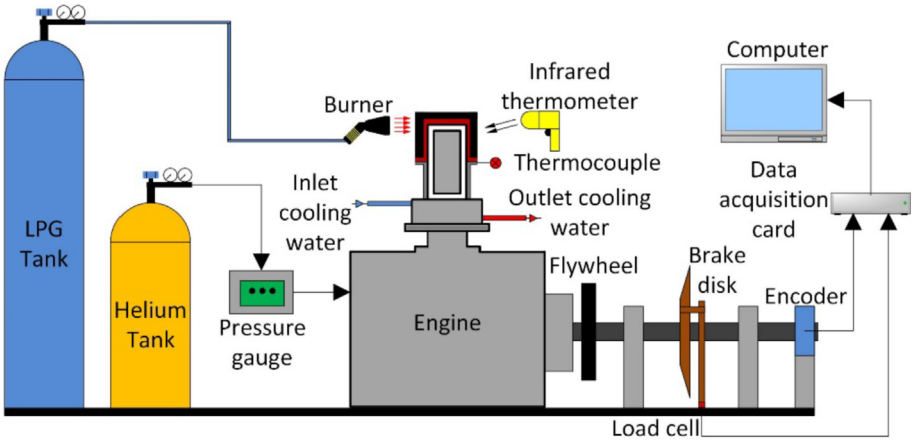

Fig. 3. Schematic illustration of the experimental setup.

Table 3
Independent parameters and their levels applied for CCD design.

Independent variable	X_i	Codes factor levels				
		$-\alpha$	−1	0	+1	$+\alpha$
Engine Speed (rpm)	X_1	550	600	650	700	750
Pressure (bar)	X_2	5	6	7	8	9
Temperature (°C)	X_3	600	600	–	700	700

$$DF = \left((df_1)^{p_1}(df_2)^{p_2}\ldots(df_n)^{p_n}\right)^{\frac{1}{\sum p_i}} = \left(\prod_{i=1}^{n} df_i^{p_i}\right)^{\frac{1}{\sum p_i}} \quad (2)$$

where df_1, $df_2 \ldots df_n$ are the overall desirability of the process, n is the number of the outputs in the experiment, and *Pi* is the importance of each factor. In this study, the goals of maximum and minimum were obtained to define the desirability function (df_i) by using Eq. (3) and Eq. (4), respectively [60].

$$df_i = \begin{cases} 0 & y_i \le w_i^{min} \\ \left(\dfrac{y_i - w_i^{min}}{w_i^{max} - w_i^{min}}\right)^{w_i} & w_i^{min} \le y_i \le w_i^{max} \\ 1 & y_i \ge w_i^{max} \end{cases} \quad (3)$$

$$df_i = \begin{cases} 1 & y_i \le w_i^{min} \\ \left(\dfrac{w_i^{max} - y_i}{w_i^{max} - w_i^{min}}\right) w^i & w_i^{min} \le y_i \le w_i^{max} \\ 0 & y_i \ge w_i^{max} \end{cases} \quad (4)$$

where y_i is the ith response value, w_i^{max} and w_i^{min} are maximum and minimum values for the response, respectively. The goal of optimization was to find a set of engine working conditions that meet maximum desirability function in the range of input parameters.

3. Results and discussion

3.1. The effects of charge pressure, temperature, and engine speed on the brake power

Fig. 5 show the power variations of the prototype engine for different charge pressures of the working fluid and hot end temperatures of 500, 600, and 700 °C.

As depicted in Fig. 5, unloaded engine speed reached over 1000 rpm with 700 °C hot end temperature and charge pressure of 9 bar. As illustrated in Fig. 5, the engine torque had a maximum value at a particular value of engine speed. Higher engine speed clearly led to limited heating/cooling time, and subsequently leading to inadequate heat transfer. Besides, a further increase in engine speed over the optimum value causes a decrease in brake power. A similar trend was also reported by Karabulut et al. [71]. Their results illustrated that maximum power output was reported at charge pressure of 2.8 bars and an engine speed of 453 rpm. In a different investigation, Karabulut et al. [72] reported that shaft power of 51.93 W could be achieved by using hot-end temperature of 200 °C, charge pressure of 2.8 bar, and the engine speed of 453 rpm.

Table 4 indicates the analysis of variance (ANOVA) for the brake power.

According to Table 4, the P-value of the model was less than 0.01,

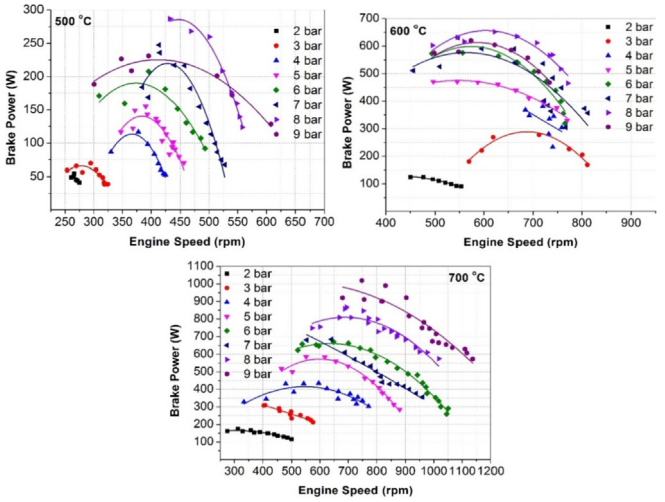

Fig. 5. Variation of the engine power with respect to engine speed at 500, 600, and 700 °C of hot end temperatures.

Table 4
ANOVA table for engine power.

Source	Sum of square	Mean square	F-value	P-value
Model	2.957E+5	18483.31	51.39	< 0.0001
X_1	24611.33	24611.33	68.43	< 0.0001
X_2	64335.79	64335.79	178.88	< 0.0001
X_3	40674.19	40674.19	113.09	< 0.0001
$X_2 \times X_3$	11572.38	11572.38	32.18	0.0003
X^2_1	7089.53	7089.53	19.71	0.0016
$X^2_2 \times X_1$	9942.1	9942.91	27.65	0.0005
$X^2_2 \times X_3$	9463.98	9463.98	26.31	0.0006
$X^2_2 \times X_3 \times X_1$	2492.93	2492.93	6.93	0.027
$X^2_1 \times X^2_2$	10601.6	10601.6	29.48	0.0004
Lack of Fit	363.72	359.15	1.01	0.34
Residual	3236.95	359.66		

indicating the model is significant. Ideally, a p-value less than 0.05, indicating the quantitative model is statistically significant and acceptable. In addition, the corresponding R-squared is 0.9982 for the model and it indicates that the mode provided has a large value of goodness-of-fit. Accordingly, the ANOVA results show that variables X_1 Engine Speed (p-value <0.0001), X_2 Pressure (p-value <0.0001), and X_3 temperatures are all significant parameters for the engine brake power.

With consideration of Table 3 and the Eq. (1), the quadratic model expressed by Eq. (2) was derived, representing the brake power as a function of independent variables. The large value of adjusted R^2 (0.98) for Eq. (2) demonstrate that the model was able to predict the response with good accuracy.

$$\begin{aligned} Power\ (W) = {} & 627.34 - 39.22\,X_1 + 63.41X_2 + 59.21X_3 \\ & + 26.89X_2X_3 - 12.45X_1^2 + 43.18X_2^2X_1 + 14.37X_2^2X_3 \\ & + 43.84X_1^2X_2^2 + 21.62X_1X_3\,X_2^2 \end{aligned} \quad (5)$$

From the suggested model (Eq. (2)), it is possible to derive the optimal parameters maximizing the brake power. The interaction engine power with different engine speeds and charge pressure of the rhombic drive Stirling engine were illustrated in Fig. 6a and b. As shown in Fig. 6a, by increasing the engine speed from 550 to 650 rpm, the brake power first followed a dropping trend. When the power traces were examined, it was seen that the brake power increased with the engine speed and then started to decrease after

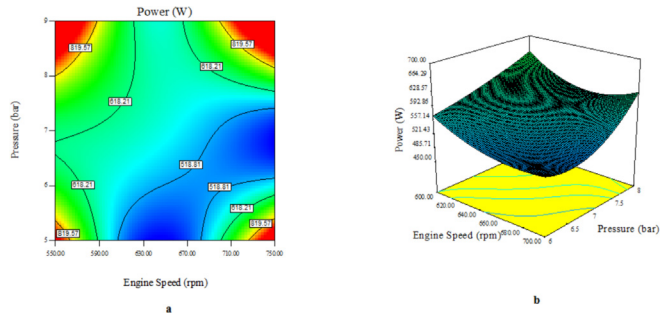

Fig. 6. (a) 2D and (b) 3D representations of the interactions of Engine speed and pressure on engine power.

reaching its maximum for almost each hot end temperature and charge pressure. At low engine speeds, heat loss to the cooler and the other parts such as piston, displacer, and engine block and gas leakage between piston and cylinder are high because there is plenty of time interval to complete a cycle. As depicted in Fig. 6b, as the engine speed increase, these losses reduce, and as a result, engine power increases. The reasons for the power decrease at higher engine speeds are the insufficient time for heating working fluid, increased pressure loss due to deteriorated flow, especially in the regenerator section, increased mechanical losses due to the frictions. It was also seen that the speed range of the engine was enlarged with increasing charge pressures. Increasing hot end temperature from 500 to 600 °C provided 367 W power enhancement, and maximum engine power was recorded as 654 W at an engine speed of 622 rpm with a similar charge pressure of 8 bar. At 600 °C of hot-end temperature, the maximum power of the engine was 663 W in the previous design of the engine. That power output was corresponding a specific power of 957 W/L via considering the total volume of the engine. In the present design, at the same hot end temperature, the specific power of the engine was increased to 1100 W/L despite the decreased heat transfer surface area. This result proves that both engine performance and thermal efficiency were improved with the presented design. Moreover, the empirical data were analysed using response surface methodology. The peak power of the engine was obtained at 700 °C hot end temperature as 1020 W at 747 rpm with a charge pressure of 9 bar.

Cheng and Yang [48], also demonstrated that beta-type Stirling engine power is the function of the geometric parameters, the total dead volume ratio, the temperature ratio, and pressure in the chambers. The optimal value of the above-mentioned influential parameters toward the maximization of the dimensionless shaft work was reported. Ye et al. [66] also observed a similar increment rate in output power as a result of the enhancement of the charge-pressure in the chamber and the rise of hot-end temperature. Their finding indicated that the increase of the hot end temperature would increase the Stirling cycle pressure, leading to an increase in the shaft power. More specifically, they specified that charge pressure had a more remarkable effect in comparison to that of the hot end temperature.

3.2. The effects of charge pressure, temperature, and engine speed on the brake torque

Fig. 7 illustrates the brake torque variations versus engine speed for different hot end temperatures and charge pressures.

The statistical analysis results for engine torque are given in Table 5. With regard to the independent variables (temperature, pressure, and engine speed), the engine torque was significant at the 1% level. The results obtained showed that the regression model had a large value of goodness-of-fit (R-squared = 0.9888), indicating only less than 0.1% of the total variation could not be estimated by the quadratic model provided.

According to Table 5, the effect of input factors (i.e., engine speed, pressure, and temperature) was also significant (p-value <0.0001) on the engine torque level. The F-value of 49.73 and the p-value of 0.001 in regression models indicate that the quadratic model estimates the response parameters very accurately. The following quadratic model (Eq. (6)) for the engine torque was generated from the RSM-based multivariate regression analysis.

$$\text{Torque (N.m)} = 9.27 - 1.27\ X_1 + 0.88\ X_2 + 1.1\ X_3 + 0.32\ X_2X_3 - 0.13X_2^2X_3 + 067X_3^2X_1 + 0.54\ X_1^2X_2^2 \quad (6)$$

Fig. 8 indicates the 2D and 3D representations of engine torque against temperature and charge pressure. As it is expected, the maximum brake torque values were obtained at minimum engine speeds for almost each hot end temperature and charge pressure levels. This is because of the improved heating performance at low engine speeds. At the lower engine speeds, there is plenty of time to heat transfer by comparing higher engine speeds. As a result of this phenomenon maximum engine torque values are obtained at lower engine speeds in Stirling engines. According to Fig. 8, the modeling results demonstrate that, by increasing the engine speed from 600 to 700 rpm, engine torque decreases by 28%. As depicted in Figs. 7 and 8, the engine torque was rising as the charge pressure increased. At 500 and 600 °C, hot end temperatures brake torque started to decrease after 8 bar charge pressure. The Stirling engine performance is very sensitive to its operating condition [73]. Higher charge pressure levels increase the mass of the working fluid in the cylinder. If sufficient heat transfer can be provided in a limited time interval, engine performance also improves. However, too much working fluid mass may decrease engine performance if there is not sufficient heat flux. In order to prevent performance loss, hot end temperature could be increased if it is possible. When the torque traces at 700 °C are examined, it can be seen that the loss of performance is prevented in that way. According to Fig. 8a and b, the relation between engine speed and charge pressure seems to be quadratic.

These findings were in line with those of the other studies in which the variation of the shaft torque/power with respect to hot end temperature and the charge pressure were investigated. Karabulut et al. [71] reported that the performance characteristics increase with hot end temperature and the charge pressure. The maximum torque was reported as ~4 Nm at 260 °C hot end temperature and 4 bars charge pressure.

3.3. Multi-objective optimization and validation

In the present study, the desirability function approach was used to determine optimal engine working conditions, with the objective of maximizing the engine torque/engine power. Design Expert v. 10 was employed to optimize the effects of pressure, temperature, and engine speed on the performance of the Stirling engine. The desirability is shown in Fig. 9 is reasonable, considering the parameter values for the multi-objective optimization. In Fig. 9, Optimal response prediction values are displayed in red. 2-D plot for multi-responses and desirability are depicted in Fig. 9.

According to Fig. 9, at optimized values of independent parameters, the amount of engine brake power and engine torque were obtained to be 862.53 W and 11.84 Nm, respectively. The importance of 3 was considered for all parameters, and each response was weighted equally (w = 1:1:1). In this way, the desirability functions methodology was utilized to select the optimum engine working condition.

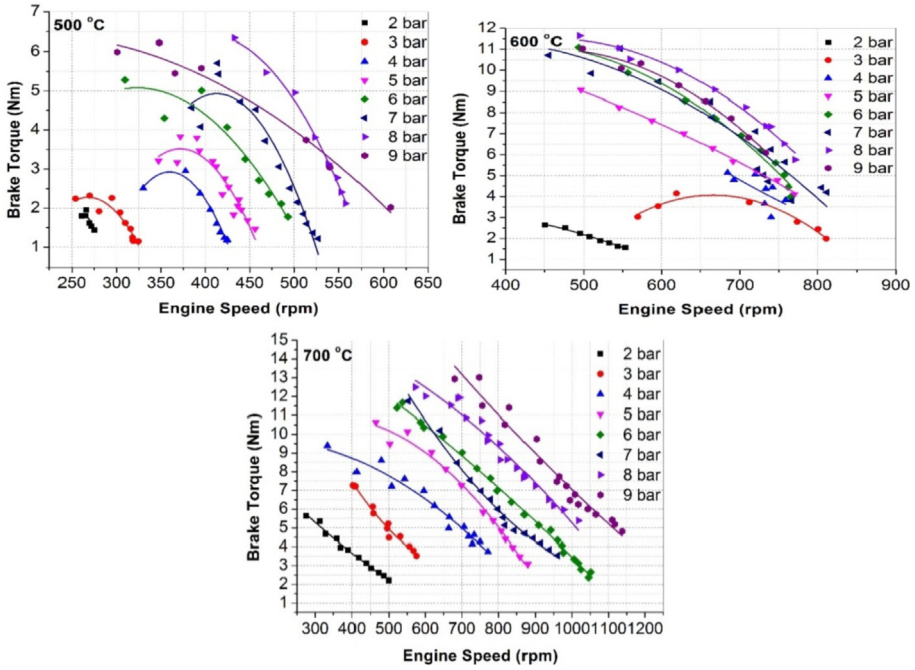

Fig. 7. Variation of the engine torque with respect to engine speed at 500, 600 and 700 °C of hot end temperatures.

Table 5
ANOVA table for engine torque.

Source	Sum of square	Mean square	F-value	P-value
Model	86.33	5.40	5.40	< 0.0001
X_1	25.86	25.86	25.86	< 0.0001
X_2	12.29	12.29	12.29	< 0.0001
X_3	13.94	13.94	13.94	< 0.0001
$X_2 \times X_3$	1.65	1.65	1.65	0.0036
$X^2_1 \times X_3$	0.8	0.8	0.8	0.0236
$X^2_2 \times X_1$	2.4	2.4	2.4	0.001
$X^2_2 \times X_3$	0.78	0.78	0.78	0.025
$X^2_1 \times X^2_2$	1.63	1.63	1.63	0.003
Lack of Fit	0.14	0.14	0.14	0.28
Residual	0.98	0.11		

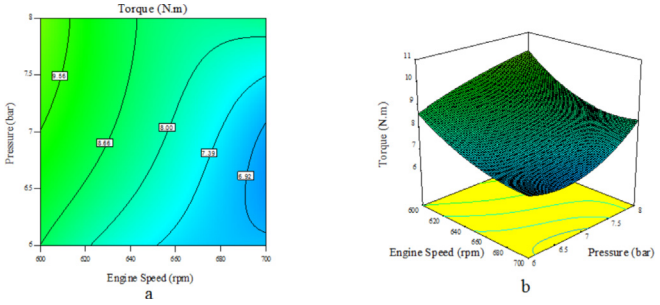

Fig. 8. (a) 2D and (b) 3D representations of the interactions of Engine speed and pressure on Torque.

Table 6 illustrates the lower/upper limits, weight, and the importance of each independent and response parameters.

According to the constraints above, the optimal engine speed, charge pressure, charge pressure were 700 rpm, 8 bar, and 700 °C, respectively, with the desirability of 0.86. In order to evaluate the accuracy of the model, an experimental validation was also carried out under optimum conditions. In this condition, the Stirling engine provided 11.95 Nm and 868.13. The difference between optimization and the experimental result indicates that the RSM models are reliable and accurate with respect to the engine performance characteristics, with an absolute error of less than 4%. This error can be due to a lack of experimental measurement resulting in a lack of combined desirability values.

A similar finding was also reported by other researchers when the multi-response optimization was used to obtain an optimal response of various Stirling engine operating conditions. For instance, Ye et al. [66] reported that the desirability approach could be employed to predict the output power, thermal and exergy efficiency of the Stirling engine. Their findings showed that charge pressure of 3.98 MPa, hot end and cold end temperature of 920 K and 330.3 K were found to be the optimal value. The corresponding thermal and output power were reported as 38% and 137 W, respectively. Also, their errors reported (i.e. 0.37%) were in agreement with the findings of the present work. Similar results were also reported in a different study conducted by Cheng and Yang [48] who investigated influential factors affecting the output power in a beta-type Stirling engine. They reported that prediction deviations for the experimental data and predicted results were within 5.2%.

As mentioned above, the present work covered the CCD-based RSM method for optimizing the Stirling engine parameters. However, Improvement of the performances of multi-objective optimization algorithms continues to be the focus of much research. it is suggested that future research on the optimization of the Stirling engine use a hybrid algorithm by combining RSM with other optimization methods including, adaptive-network-based fuzzy inference system (ANFIS), artificial neural network approach (ANN), and GA (genetic algorithm) to improve the RSM-based algorithm compared with previous studies on the Stirling engine.

4. Conclusion

In the present study, the effects of operating parameters such as heating temperature, charge pressure, and engine speed are investigated and optimized by CCD based RSM method for a beta-

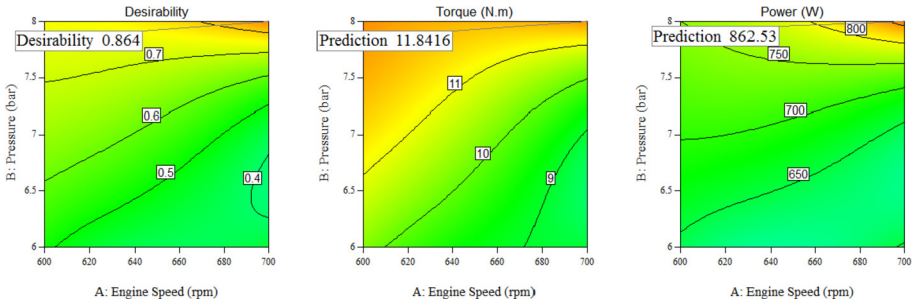

Fig. 9. 2D plot for responses and desirability.

Table 6
The multi-objective constraints.

Factors	Goal	Upper limit	Lower limit	Upper weight	Lower weight	Importance
A: Engine Speed	In range	750	550	1	1	3
B: Pressure	In range	9	9	1	1	3
C: Temperature	In range	700	600	1	1	3
Brake power	Maximize	921.08	439.64	1	1	3
Brake torque	Maximize	12.94	5.65	1	1	3

type rhombic drive Stirling engine. The engine used in this study was manufactured and tested in a previous study and it was provided 957 W/L specific engine power. Another goal of the present study was to enhance the specific power of the engine by increasing the compression ratio. Displacer cylinder and the displacer lengths were shortened and the compression ratio was increased from 2.51 to 2.76. Although the reduced heat transfer surface area due to shortening the displacer cylinder, specific power increased 13% and recorded as 1100 W/L. C was employed to analyze the statistical significance and the effect of independent parameters (i.e. engine speed, charge pressure, and temperature) on the output brake power and engine torque. The results illustrated that:

(1) The regression models for the engine brake power and engine torque are developed. The ANOVA was employed to find the best quadratic regression model. The results obtained showed that all independent factors have significant impacts on the performance characteristic of the Stirling engine.
(2) The interactive effect of the input variables which had a significant effect (p-value <0.0001) on the output brake power and engine torque were depicted in detail. Moreover, the effect of the input parameters on the response variables was determined using the statistical results of predicted models. The p-values and F-values of the quadratic models illustrated that model-derived were statistically significant for both response parameters, indicating the effectiveness of multi-objective optimization.
(3) The maximum power of the engine was recorded at 700 °C hot end temperature as 1020 W at 747 rpm with a charge pressure of 9 bar.
(4) An engine speed of 700 rpm and a charge pressure of 8 bar and heating temperature of 700 °C were found to be optimal values. The results of this study indicated that at optimal engine working conditions, the amounts of the brake torque and brake power were found to be 11.95 Nm and 868.13 W, respectively. While the end temperature is varying from 500 °C to 600 °C, the engine power increases up to 654W at an engine speed of 622 rpm and charge pressure of 8 bar.
(5) The errors obtained between experiments data and predicted values of RSM for brake power and engine torque was less than 4%, indicating high accuracy of the optimal results.
(6) Desirability approach based RSM was employed as a reliable technique to optimize the performance of a beta-type Stirling engine. The outcomes of the study could effectively be implemented for efficient designing Stirling engine performance and further optimizing its performance.

Declaration of competing interest

The authors declare that they have no known competing financial interests or personal relationships that could have appeared to influence the work reported in this paper.

CRediT authorship contribution statement

Hamit Solmaz: Supervision, Conceptualization, Methodology, Writing - original draft, Project administration. **Seyed Mohammad Safieddin Ardebili:** Methodology, Software, Writing - original draft, Writing - review & editing. **Fatih Aksoy:** Project administration, Funding acquisition, Conceptualization. **Alper Calam:** Validation, Investigation, Writing - review & editing. **Emre Yılmaz:** Validation, Investigation, Writing - review & editing. **Muhammed Arslan:** Writing - original draft.

Acknowledgment

This study was supported by TUBITAK in frame of the project code of 113M192 as researchers, we thank the TUBITAK.

References

[1] Aghbashlo M, Tabatabaei M, Khalife E, Roodbar Shojaei T, Dadak A. Exergoeconomic analysis of a DI diesel engine fueled with diesel/biodiesel (B5) emulsions containing aqueous nano cerium oxide. Energy 2018;149:967–78. https://doi.org/10.1016/j.energy.2018.02.082.
[2] Aghbashlo M, Tabatabaei M, Mohammadi P, Khoshnevisan B, Rajaeifar MA, Pakzad M. Neat diesel beats waste-oriented biodiesel from the exergoeconomic and exergoenvironmental point of views. Energy Convers Manag 2017;148:1–15. https://doi.org/10.1016/j.enconman.2017.05.048.
[3] Calam A, Solmaz H, Yılmaz E, İçingür Y. Investigation of effect of compression ratio on combustion and exhaust emissions in A HCCI engine. Energy 2019;168:1208–16. https://doi.org/10.1016/j.energy.2018.12.023.
[4] Kocakulak T, Solmaz H. Elektrikli bir aracın modellenmesi ve rejeneratif fren sisteminin bulanık mantık yöntemi ile kontrol edilmesi. Int. Symp. Automot.

Sci. Technol. 2019;(1):582–92.
[5] Kocakulak T, Solmaz H. Buji ile ateşlemeli motor kullanılan seri hibrit elektrikli bir aracın modellenmesi. Proc. Int. Conf. Technol. Sci. 2018;1:353–60.
[6] Tabanlıgil Calam T. Analytical application of the poly(1H-1,2,4-triazole-3-thiol) modified gold electrode for high-sensitive voltammetric determination of catechol in tap and lake water samples. Int J Environ Anal Chem 2019;99:1298–312. https://doi.org/10.1080/03067319.2019.1619716.
[7] Tabanlıgil Calam T. 1H-1, 2, 4-triazole-3-thiol modifiye altın elektrot kullanılarak fenolün elektrokimyasal davranışının incelenmesi ve volta835metrik tayini. Gazi Üniversitesi Mühendislik-Mimarlık Fakültesi Derg 2020;35:835–44. https://doi.org/10.17341/gazimmfd.543608.
[8] Ran Z, Hariharan D, Lawler B, Mamalis S. Exploring the potential of ethanol, CNG, and syngas as fuels for lean spark-ignition combustion - an experimental study. Energy 2020;191:116520. https://doi.org/10.1016/j.energy.2019.116520.
[9] Nuthan Prasad BS, Pandey JK, Kumar GN. Impact of changing compression ratio on engine characteristics of an SI engine fueled with equi-volume blend of methanol and gasoline. Energy 2020;191:116605. https://doi.org/10.1016/j.energy.2019.116605.
[10] Nautiyal P, Subramanian KA, Dastidar MG, Kumar A. Experimental assessment of performance, combustion and emissions of a compression ignition engine fuelled with Spirulina platensis biodiesel. Energy 2020;193:116861. https://doi.org/10.1016/j.energy.2019.116861.
[11] Aghbashlo M, Tabatabaei M, Mohammadi P, Pourvosoughi N, Nikbakht AM, Goli SAH. Improving exergetic and sustainability parameters of a Di diesel engine using polymer waste dissolved in biodiesel as a novel diesel additive. Energy Convers Manag 2015;105:328–37. https://doi.org/10.1016/j.enconman.2015.07.075.
[12] Rosen MA. Environmental sustainability tools in the biofuel industry. Biofuel Res J 2018;5:751–2. https://doi.org/10.18331/BRJ2018.5.1.2.
[13] Kıyaklı AO, Solmaz H. Modeling of an electric vehicle with MATLAB/simulink. Int J Automot Sci Technol 2019;2:9–15. https://doi.org/10.30939/ijastech..475477.
[14] Rather MA, Wani MM. A numerical study on the effects of exhaust gas recirculation temperature on controlling combustion and emissions of a diesel engine running on HCCI combustion mode. Int J Automot Sci Technol 2018;2:17–27. https://doi.org/10.30939/ijastech..451574.
[15] Sezer İ. A review study on the using of diethyl ether in diesel engines: effects on CO emissions. Int J Automot Sci Technol 2019;3:6–20. https://doi.org/10.30939/ijastech..507799.
[16] Wenming Y, Meng Y. Phi-T map analysis on RCCI engine fueled by methanol and biodiesel. Energy 2019;187:115958. https://doi.org/10.1016/j.energy.2019.115958.
[17] Uyumaz A, Solmaz H. The effects of inlet air temperature and premixed fuel ratio on RCCI combustion and engine performance characteristics. J Polytech Derg 2017;20:689–98.
[18] Polat S, Uyumaz A, İpci D, Yücesu HS, Solmaz H, Yılmaz E. Doğalgaz yakıtlı HCCI bir motorda hidrojen İlavesinin yanma karakteristikleri üzerindeki etkilerinin nümerik olarak i?ncelenmesi. Makine Teknol Elektron Derg 2015;12:15–26.
[19] Polat S, Solmaz H, Calam A, Yılmaz E. Estimation of the COVIMEP variation in a HCCI engine. J Polytech Derg 2020. https://doi.org/10.2339/politeknik.567865.
[20] Halis S, Nacak Ç, Solmaz H, Yılmaz E, Yücesu HS. Investigation of the effects of octane number on combustion characteristics and engine performance in a HCCI engine. Isi Bilim Ve Tek Dergisi-Journal Therm Sci Technol 2018;38:99–110.
[21] Chahartaghi M, Sheykhi M. Energy, environmental and economic evaluations of a CCHP system driven by Stirling engine with helium and hydrogen as working gases. Energy 2019;174:1251–66. https://doi.org/10.1016/j.energy.2019.03.012.
[22] Abuelyamen A, Ben-Mansour R, Abualhamayel H, Mokheimer EMA. Parametric study on beta-type Stirling engine. Energy Convers Manag 2017;145:53–63. https://doi.org/10.1016/j.enconman.2017.04.098.
[23] Hachem H, Gheith R, Aloui F, Ben Nasrallah S. Technological challenges and optimization efforts of the Stirling machine: a review. Energy Convers Manag 2018;171:1365–87. https://doi.org/10.1016/j.enconman.2018.06.042.
[24] Ahmadi MH, Ahmadi MA, Pourfayaz F. Thermal models for analysis of performance of Stirling engine: a review. Renew Sustain Energy Rev 2017;68:168–84. https://doi.org/10.1016/j.rser.2016.09.033.
[25] Güven M, Bedir H, Anlaş G. Optimization and application of Stirling engine for waste heat recovery from a heavy-duty truck engine. Energy Convers Manag 2019;180:411–24. https://doi.org/10.1016/j.enconman.2018.10.096.
[26] Cheng CH, Chen YF. Numerical simulation of thermal and flow fields inside a 1-kW beta-type Stirling engine. Appl Therm Eng 2017;121:554–61. https://doi.org/10.1016/j.applthermaleng.2017.04.105.
[27] Caetano BC, Lara IF, Borges MU, Sandoval OR, Valle RM. A novel methodology on beta-type Stirling engine simulation using CFD. Energy Convers Manag 2019;184:510–20. https://doi.org/10.1016/j.enconman.2019.01.075.
[28] Ahmadi MH, Ahmadi MA, Mellit A, Pourfayaz F, Feidt M. Thermodynamic analysis and multi objective optimization of performance of solar dish Stirling engine by the centrality of entransy and entropy generation. Int J Electr Power Energy Syst 2016;78:88–95. https://doi.org/10.1016/j.ijepes.2015.11.042.
[29] Eid EI, Khalaf-Allah RA, Soliman AM, Easa AS. Performance of a beta Stirling refrigerator with tubular evaporator and condenser having inserted twisted tapes and driven by a solar energy heat engine. Renew Energy 2019;135:1314–26. https://doi.org/10.1016/j.renene.2018.09.044.
[30] Erol D, Yaman H, Doğan B. A review development of rhombic drive mechanism used in the Stirling engines. Renew Sustain Energy Rev 2017;78:1044–67. https://doi.org/10.1016/j.rser.2017.05.025.
[31] Çınar C, Aksoy F, Solmaz H, Yılmaz E, Uyumaz A. Manufacturing and testing of an A-type Stirling engine. Appl Therm Eng 2018;130:1373–9. https://doi.org/10.1016/j.applthermaleng.2017.11.132.
[32] Bataineh K. Mathematical formulation of alpha -type Stirling engine with Ross Yoke mechanism. Energy 2018;164:1178–99. https://doi.org/10.1016/j.energy.2018.08.134.
[33] Altin M, Okur M, Ipci D, Halis S, Karabulut H. Thermodynamic and dynamic analysis of an alpha type Stirling engine with Scotch Yoke mechanism. Energy 2018;148:855–65. https://doi.org/10.1016/j.energy.2018.01.183.
[34] Shufat SA, Kurt E, Cinar C, Aksoy F, Hançerlioğulları A, Solmaz H. Exploration of a Stirling engine and generator combination for air and helium media. Appl Therm Eng 2019;150:738–49. https://doi.org/10.1016/j.applthermaleng.2019.01.053.
[35] Thombare DG, Verma SK. Technological development in the Stirling cycle engines. Renew Sustain Energy Rev 2008;12:1–38. https://doi.org/10.1016/j.rser.2006.07.001.
[36] Almajri AK, Mahmoud S, Al-Dadah R. Modelling and parametric study of an efficient Alpha type Stirling engine performance based on 3D CFD analysis. Energy Convers Manag 2017;145:93–106. https://doi.org/10.1016/j.enconman.2017.04.073.
[37] Aksoy F, Cinar C. Thermodynamic analysis of a beta-type Stirling engine with rhombic drive mechanism. Energy Convers Manag 2013;75:319–24. https://doi.org/10.1016/j.enconman.2013.06.043.
[38] Cheng CH, Yu YJ. Numerical model for predicting thermodynamic cycle and thermal efficiency of a beta-type Stirling engine with rhombic-drive mechanism. Renew Energy 2010;35:2590–601. https://doi.org/10.1016/j.renene.2010.04.002.
[39] Solmaz H, Karabulut H. Performance comparison of a novel configuration of beta-type Stirling engines with rhombic drive engine. Energy Convers Manag 2014;78:627–33. https://doi.org/10.1016/j.enconman.2013.11.028.
[40] Aksoy F, Solmaz H, Karabulut H, Cinar C, Ozgoren YO, Polat S. A thermodynamic approach to compare the performance of rhombic-drive and crank-drive mechanisms for a beta-type Stirling engine. Appl Therm Eng 2016;93:359–67. https://doi.org/10.1016/j.applthermaleng.2015.09.105.
[41] Gultekin E, Cinar C, Okur M. Design, manufacturing and testing of a prototype two-stroke engine with rhombic drive mechanism. Int J Environ Sci Technol 2020;17:455–62. https://doi.org/10.1007/s13762-019-02488-z.
[42] Cheng CH, Huang CY, Yang HS. Development of a 90-K beta type Stirling cooler with rhombic drive mechanism. Int J Refrig 2019;98:388–98. https://doi.org/10.1016/j.ijrefrig.2018.11.027.
[43] Cheng CH, Yu YJ. Combining dynamic and thermodynamic models for dynamic simulation of a beta-type Stirling engine with rhombic-drive mechanism. Renew Energy 2012;37:161–73. https://doi.org/10.1016/j.renene.2011.06.013.
[44] Erol D. Stirling motorlarında kullanılan hareket i?letim mekanizmaları. Electron J Veh Technol 2011;3:51–74.
[45] Walker G. Stirling engines. 1980.
[46] Shendage DJ, Kedare SB, Bapat SL. An analysis of beta type Stirling engine with rhombic drive mechanism. Renew Energy 2011;36:289–97. https://doi.org/10.1016/j.renene.2010.06.041.
[47] El Hassani H, eddine Boutammachte N, Knorr J, El Hannaoui M. Study of a low-temperature Stirling engine driven by a rhombic drive mechanism. Int J Energy Environ Eng 2013;4:1. https://doi.org/10.1186/2251-6832-4-40.
[48] Cheng CH, Yang HS. Optimization of rhombic drive mechanism used in beta-type Stirling engine based on dimensionless analysis. Energy 2014;64:970–8. https://doi.org/10.1016/j.energy.2013.11.054.
[49] Zainudin MF, Bakar RA, Ming GL, Ali T, Sup BA. Thermodynamic cycle evaluation of rhombic drive beta-configuration Stirling engine. Energy Procedia 2015;68:419–28. https://doi.org/10.1016/j.egypro.2015.03.273.
[50] Ni M, Shi B, Xiao G, Peng H, Sultan U, Wang S, et al. Improved Simple analytical model and experimental study of a 100 W β-type stirling engine. Appl Energy 2016;169:768–87. https://doi.org/10.1016/j.apenergy.2016.02.069.
[51] Badr WS, Fanni M, Abdel-Rahman AK, Rasoul SA. Dynamic simulation and optimization of rhombic drive stirling engine using MSC ADAMS software. Procedia Technol 2016;22:754–61. https://doi.org/10.1016/j.protcy.2016.01.035.
[52] Xiao G, Sultan U, Ni M, Peng H, Zhou X, Wang S, et al. Design optimization with computational fluid dynamic analysis of β-type Stirling engine. Appl Therm Eng 2017;113:87–102. https://doi.org/10.1016/j.applthermaleng.2016.10.063.
[53] Yang HS, Cheng CH. Development of a beta-type Stirling engine with rhombic-drive mechanism using a modified non-ideal adiabatic model. Appl Energy 2017;200:62–72. https://doi.org/10.1016/j.apenergy.2017.05.075.
[54] Yang HS, Cheng CH, Huang ST. A complete model for dynamic simulation of a 1-kW class beta-type Stirling engine with rhombic-drive mechanism. Energy 2018;161:892–906. https://doi.org/10.1016/j.energy.2018.07.159.
[55] Mohammadi MA, Jafarian A. CFD simulation to investigate hydrodynamics of oscillating flow in a beta-type Stirling engine. Energy 2018;153:287–300. https://doi.org/10.1016/j.energy.2018.04.017.
[56] Ahmed F, Hulin H, Khan AM. Numerical modeling and optimization of beta-

type Stirling engine. Appl Therm Eng 2019;149:385–400. https://doi.org/10.1016/j.applthermaleng.2018.12.003.
[57] El-Ghafour SA, El-Ghandour M, Mikhael NN. Three-dimensional computational fluid dynamics simulation of stirling engine. Energy Convers Manag 2019;180:533–49. https://doi.org/10.1016/j.enconman.2018.10.103.
[58] Cheng CH, Yang HS, Keong L. Theoretical and experimental study of a 300-W beta-type Stirling engine. Energy 2013;59:590–9. https://doi.org/10.1016/j.energy.2013.06.060.
[59] Safieddin Ardebili SM, Taghipoor A, Solmaz H, Mostafaei M. The effect of nano-biochar on the performance and emissions of a diesel engine fueled with fusel oil-diesel fuel. Fuel 2020;268:117356. https://doi.org/10.1016/j.fuel.2020.117356.
[60] Safieddin Ardebili SM, Solmaz H, Mostafaei M. Optimization of fusel oil – gasoline blend ratio to enhance the performance and reduce emissions. Appl Therm Eng 2019;148:1334–45. https://doi.org/10.1016/j.applthermaleng.2018.12.005.
[61] Hassan Pour A, Safieddin Ardebili SM, Sheikhdavoodi MJ. Multi-objective optimization of diesel engine performance and emissions fueled with diesel-biodiesel-fusel oil blends using response surface method. Environ Sci Pollut Res 2018;25:35429–39. https://doi.org/10.1007/s11356-018-3459-z.
[62] Singh Y, Sharma A, Tiwari S, Singla A. Optimization of diesel engine performance and emission parameters employing cassia tora methyl esters-response surface methodology approach. Energy 2019;168:909–18. https://doi.org/10.1016/j.energy.2018.12.013.
[63] Najafi G, Ghobadian B, Yusaf T, Ardebili SMS, Mamat R. Optimization of performance and exhaust emission parameters of a SI (spark ignition) engine with gasolineeethanol blended fuels using response surface methodology. Energy 2015;90:1815–29. https://doi.org/10.1016/j.energy.2015.07.004.
[64] Dvorak TM, Hoekstra RL. Optimizing internal combustion engine performance through response surface methodology. SAE Tech Pap 1996:962525.
[65] Gheith R, Aloui F, Ben Nasrallah S. Optimization of Stirling engine performance based on an experimental design approach. Int J Energy Res 2013;37:1519–28. https://doi.org/10.1002/er.2964.
[66] Ye W, Yang P, Liu Y. Multi-objective thermodynamic optimization of a free piston Stirling engine using response surface methodology. Energy Convers Manag 2018;176:147–63. https://doi.org/10.1016/j.enconman.2018.09.011.
[67] Aksoy F, Solmaz H, Çınar C, Karabulut H. 1.2kW beta type Stirling engine with rhombic drivemechanism. Int J Energy Res 2017;41:1310–21. https://doi.org/10.1002/er.3714.
[68] Ann MA. Experimental methods for engineers: JP Holman. New York: McGraw-Hill; 1994.
[69] Sharma A, Ansari NA, Pal A, Singh Y, Lalhriatpuia S. Effect of biogas on the performance and emissions of diesel engine fuelled with biodiesel-ethanol blends through response surface methodology approach. Renew Energy 2019;141:657–68. https://doi.org/10.1016/j.renene.2019.04.031.
[70] Sakthivel R, Ramesh K, Joseph John Marshal S, Sadasivuni KK. Prediction of performance and emission characteristics of diesel engine fuelled with waste biomass pyrolysis oil using response surface methodology. Renew Energy 2019;136:91–103. https://doi.org/10.1016/j.renene.2018.12.109.
[71] Karabulut H, Çınar C, Oztürk E, Yücesu HS. Torque and power characteristics of a helium charged Stirling engine with a lever controlled displacer driving mechanism. Renew Energy 2010;35:138–43. https://doi.org/10.1016/j.renene.2009.04.023.
[72] Karabulut H, Yücesu HS, Çınar C. Nodal analysis of a Stirling engine with concentric piston and displacer. Renew Energy 2006;31:2188–97. https://doi.org/10.1016/j.renene.2005.12.009.
[73] Gheith R, Aloui F, Ben Nasrallah S. Study of temperature distribution in a Stirling engine regenerator. Energy Convers Manag 2014;88:962–72. https://doi.org/10.1016/j.enconman.2014.09.043.
[74] Özsezen AN. Experimental analysis of performance, combustion and injection characteristics of biodiesels obtained from waste cooking and canola oils. Int J Automot Sci Technol 2017;1(1):22–8.
[75] Sezer İ. A review study on the using of diethyl ether in diesel engines: Effects on CO emissions. Int J Automot Sci Technol 2019;3(1):6–20. https://doi.org/10.30939/ijastech..507799.
[76] Ciniviz M, Örs İ, Sayın Kul B. The effect of adding EN (2-Ethylhexyl Nitrate) to diesel-ethanol blends on performance and exhaust emissions. Int J Automot Sci Technol 2017;1(1):16–21.
[77] Uyumaz A, Aksoy F, Boz F, Yılmaz E. Experimental investigation of neutralized waste cooking oil biodiesel and diesel fuels in a direct injection diesel engine at different engine loads. Int J Automot Sci Technol 2017;1(1):7–15.